Available online at www.sciencedirect.com
ScienceDirect
Journal of Photochemistry and Photobiology A: Chemistry 197 (2008) 245–252
Journal of Photochemistry and Photobiology A:Chemistry
www.elsevier.com/locate/jphotochem

Ultraviolet stimulation of hydrogen peroxide production using aminoindazole, diaminopyridine, and phenylenediamine solid polymer complexes of Zn(II)

J.A. Hayes [a], D.M. Schubert [b], J.E. Amonette [a], P. Nachimuthu [a], R.S. Disselkamp [a,*]

[a] *Institute for Interfacial Catalysis, Pacific Northwest National Laboratory, Richland, WA 99352, United States*
[b] *Rio Tinto Minerals, Greenwood Village, CO 80111, United States*

Received 11 October 2007; received in revised form 17 December 2007; accepted 28 December 2007
Available online 5 January 2008

Abstract

Hydrogen peroxide (H_2O_2) is a valuable chemical commodity whose production relies on expensive and energy intensive methods. If an efficient, sustainable, and inexpensive solar-mediated production method could be developed from the reaction between dioxygen and water then the use of H_2O_2 as a fuel may be possible and gain acceptance. When concentrated at greater than 10 M, H_2O_2 possesses a high specific energy, is environmentally clean, and is easily stored. However, the current method of manufacturing H_2O_2 via the anthraquinone process is environmentally unfriendly making the unexplored nature of its photochemical production at high concentration from solar irradiation of interest. Towards this end, we studied the concentration and quantum yield of hydrogen peroxide produced in an ultraviolet (UV-B) irradiated environment using solid, Zn(II)-centered, complexes of amino-substituted isomers of indazole, pyridine, and phenylenediamine to catalyze the reaction. Aqueous suspensions in contact with air were exposed to 280–360-nm light from a low-power lamp. Of the ten complexes studied, Zn-5-aminoindazole had the greatest first-day production of 63 mM/day with a 37% quantum yield and *p*-phenylenediamine (PPAM) showed the greatest long-term stability. Isomeric forms of the catalysts' organic components (e.g., amino groups) affected H_2O_2 production. For example, irradiation of diaminopyridine isomers indicated 2,3-diamino and 3,4-diamino structures were the most productive, each generating 32 mM/day H_2O_2, whereas the 2,5-diamino isomer generated no H_2O_2. A significant decrease in H_2O_2 production with time was observed for all but PPAM, suggesting the possibility of a catalyst-poisoning mechanism. We propose a reaction mechanism for H_2O_2 production based on the stability of the resonance structures of the different isomers.
Published by Elsevier B.V.

Keywords: Zn-inorganic polymers; Photochemical; Photocatalytic; Hydrogen peroxide; Alternative energy; Fuel; Solar energy

1. Introduction

Hydrogen peroxide (H_2O_2) is well-suited as an energy storage medium for many reasons. It is a stable liquid in absence of a catalyst, only slightly toxic or corrosive at concentrations below ~10 M, portable in plastic containers, and contains a high energy density [1]. The controlled release of the energy stored in H_2O_2 can follow several paths. When mixed with a fuel, such as kerosene [2] or sugar [3], H_2O_2 can be used as a bipropellant to create a high specific power source. At high concentration, it can be catalytically decomposed into steam and dioxygen and its energy used in a turbine for power generation [4,5]. In another potential utilization process yet to be fully demonstrated, H_2O_2 is electrolyzed into pure hydrogen (at cathode) and oxygen (at anode) gas streams [6] that are subsequently used in high-power-density H_2/H_2O_2 fuel cells [7,8]. For this potential process, the energy diagram shown in Scheme 1 describes an idealized release of hydrogen peroxides power into water according to its standard-state free-energy diagram [9]. Clearly for use as an energy storage medium, it is desirable to produce H_2O_2 in as high a concentration as possible.

The anthraquinone process for H_2O_2 production, developed originally in the 1940's, has been the industry standard by which other production methods are measured [10]. This route which

* Corresponding author at: Pacific Northwest National Laboratory, 3335 Q Avenue, P.O. Box 999, MS K8-93, Richland, WA 99352, United States.
Tel.: +1 509 376 8209; fax: +1 509 376 5106.
E-mail address: robert.disselkamp@pnl.gov (R.S. Disselkamp).

1010-6030/$ – see front matter. Published by Elsevier B.V.
doi:10.1016/j.jphotochem.2007.12.031

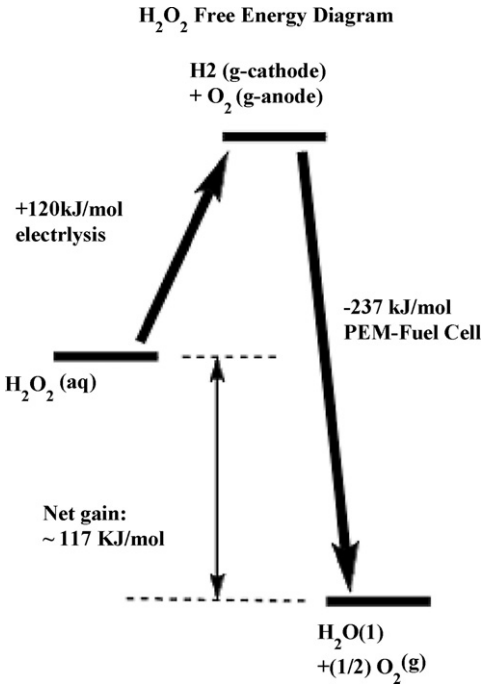

Scheme 1.

produces 95% of the global H_2O_2 supply contains a solvent extraction and hydrogenation catalyst regeneration step, making it both environmentally unfriendly and energy inefficient. Additional synthetic pathways include the dioxygen oxidation of alcohols (Shell process) to yield an aldehyde or ketone plus H_2O_2 product. A disadvantage of this method is the high alcohol solubility in H_2O_2 yielding a low purity product. A final process pioneered by Dow is the electrochemical synthesis having an energy efficiency of 95%, albeit still requiring energy. Clearly if a photocatalytic (i.e., solar-assisted) process from H_2O plus O_2 reagents is discovered then this green energy source would be the most desirable.

The most common photocatalytic method for producing H_2O_2 is to irradiate aqueous aerated suspensions of metal oxide semiconductor materials, such as TiO_2 [10], ZnO [11,12], and Sb_2O_3 [13]. For ZnO, a quantum yield of 0.25 was reported with UV irradiation [10] suggesting that, in principle, a high efficiency for H_2O_2 generation exists. However, maximum achievable steady-state H_2O_2 concentrations are relatively low. Recent work [14] has demonstrated a maximum steady-state concentration of about 1 mM H_2O_2 for ZnO.

To our knowledge, concentrations greater than 1 mM produced from pure (e.g., non-doped) aqueous material suspensions have not been reported in the literature. If the goal is to produce the maximum production rate and steady-state concentration of H_2O_2 from sunlight, then metal oxides that absorb at less than 380 nm will not overlap well with the solar actinic flux and limit H_2O_2 production ability. It is interesting to note that much of the earlier work on the H_2O_2-producing ability of irradiated aqueous oxides was motivated by these systems relevance in the atmosphere and surface soil environments [11–15]. It should be no surprise then that solar-mediated processes have the potential to have large formation rates and achievable steady-state concentrations for H_2O_2 in systems molecularly tailored to optimize these properties. The lack of prior research in attempting to form large concentrations of H_2O_2 in (simulated) solar systems serves as motivation for the present work.

Here we report on the first use of Zn(II)-centered solid-polymer catalysts to produce H_2O_2 by a photocatalytic process. Although we used ultraviolet radiation to demonstrate their utility relative to the oxides, these compounds absorb light at longer wavelengths than metal oxide semiconductors (e.g., ZnO and Sb_2O_3) and so are better candidates for solar-mediated production of H_2O_2. With these amino-substituted indazole, pyridine, and phenylenediamine Zn complexes we demonstrate maximum H_2O_2 production levels of 63 mM/day. We also interpret the ability of certain materials to generate H_2O_2 by adopting a simple mechanism and examining the stability of resonance structures for this chemistry.

2. Experiment

2.1. Inorganic Zn-ligand synthesis and characterization

Synthesis of all the compounds used a similar approach that we outline here. Zinc nitrate, and amino-substituted indazole, pyridine, and phenylenediamine reagents were purchased from Aldrich and were of reagent grade (least purity 98%). Both concentrated H_2SO_4 and NaOH chemicals were purchased from Fisher Scientific and contained a purity of >99.8% (with low dissolved metal content). All chemicals were used as received. Water (18 MΩ/cm) had been filtered to remove organic contamination and processed using reverse osmosis.

All inorganic polymer complexes were prepared using a variation of the method of Bauman and Wang [16], in a process best described as precipitation by deprotonation via base addition. This process involves a reaction of the type: $–NH_2 + Zn^{2+} \rightarrow –NH–Zn^{1+} + H^+$, where the base addition drives production formation and the process repeated to accomplish polymerization. The first step involved is separately dissolving stoichiometric quantities of soluble Zn metal salt and the organic component in distilled water. If needed, 0.5 M NaOH was added to the organic compound to make it soluble (pH ∼ 11). Metal salt and organic solutions were then combined and 0.5 M NaOH added dropwise until precipitate formed. Typically the suspension formed by base addition remained at neutral pH. In some instances (roughly half the compounds), the addition of base to create the precipitate made the suspension alkaline (pH ∼ 9) and these suspensions were left alkaline for the duration of the study. The precipitate was filtered, washed with water or base depending on the pH of precipitation, and dried in an oven at 353 K. Powder XRD analyses were performed on a Philips X'Pert MPD diffractometer with a fixed Cu anode operating at 45 kV and 40 mA. Programmable divergence and receiving slits were employed in the incident and diffracted beam paths, respectively. The 2θ angle was calibrated using a diffraction peak from Si powder at $2\theta = 56.123^\circ$.

2.2. Photochemical apparatus

The ultraviolet light source was an ozone-free Sankyo Denki UV-B G15T8E lamp with a 3.0 W output and emission wavelengths between 280 nm and 360 nm (peak at 306 nm). Photon emission was estimated using the spectral energy distribution data for 60% output (or after 100 h lighting) provided by the Denki vendor. Sample catalysts were irradiated in vertical 7 mL silicon borate vials, 1.1 cm in diameter. Five millilitres of distilled water was added to 100 mg of catalyst, and the system was stirred to keep the catalyst uniform in solution and maintain an essential dissolved ambient oxygen concentration. We assumed that sufficient sample aeration occurs by stirring that close to the Henry's law solubility of dioxygen was present in solution (i.e., ~0.26 mM [15]). The liquid surface was 4.7 cm directly below the horizontal lamp and a total of 10 samples could be irradiated simultaneously in these experiments. Ultra-violet absorbance and percent transmittance of the photocatalyst solids were measured with a UV–vis scanning spectrophotometer (Shimadzu UV-2101PC).

The system was kept at a constant temperature (298 K) and volume (by distilled water addition to replace sample evaporation) in an enclosed light-box environment purged with fresh air flow at 100 sccm (0.14 m^3/day). We assumed no loss of H_2O_2 in our experiments and, as a consequence, our analysis underestimates the efficiency (or quantum yield) of H_2O_2 production. This is justified since our largest H_2O_2 production yield is 68 mM/day, which when combined with the Henry's law solubility of H_2O_2 in water of 10^5 M/atm [15] yields a minimum volume equivalent of 11 m^3/day needed to evaporatively lose all H_2O_2. Therefore, our estimated error is predicted to be less than 1.3% due to the large Henry's law solubility of H_2O_2.

We derived and computed the quantum efficiency of H_2O_2 production using the relations in Eqs. (1) and (2). These relationships simply relate photon flux to solution phase H_2O_2 composition change.

$$R = \frac{f}{VN_a}\int_\lambda PAQ\,d\lambda \quad (1)$$

$$\%Q\,(\text{avg}) = \frac{100R}{A'R(A_{max}, Q_{max})} \quad (2)$$

In Eq. (1) R is the measured production rate of H_2O_2 (M/s) that is related to the fractional area irradiated f (dimensionless), sample volume V (L), Avogadro's number N_a, and the integral of photon output rate of lamp $P(\lambda)$ (photons/nm s), absorptivity of powder $A(\lambda)$ (dimensionless), and quantum yield of H_2O_2 production $Q(\lambda)$ (dimensionless). $R(A_{max},Q_{max})$ is the maximum possible production rate computed by setting $A = Q = 1$, and assumes 100% photon absorbance and quantum yield. The analysis here does not distinguish between photons within the radiation band driving the photochemistry. By obtaining the three quantities of the theoretical optimal production rate from the lamp spectral output and experiment geometry (e.g., $R(A_{max},Q_{max})$) with the actual measured production rate (i.e., R) and powder absorbance fraction (i.e., A') we can define the *average* quantum yield for H_2O_2 production using Eq. (2). The dimensionless quantity A' is computed as the integral of the normalized power output P multiplied by the fractional light absorbed by the materials A of Eq. (1). The lamp output emits a total of 4.7×10^{18} photons/s (from 380 nm to 360 nm) of which 0.051% are incident upon each irradiated sample vial. Each sample irradiated under our conditions had the potential of generating 170 mM/day of H_2O_2. Based on the amount of reagents used (powder material and water) a stoichiometric production of H_2O_2 based on one Zn-organic moiety producing one H_2O_2 molecule would generate a total of ~110 mM. The minimum detection limit of H_2O_2 using this approach is ~1 mM.

2.3. Hydrogen peroxide titrations

Recognition of H_2O_2 in the samples after irradiation was detected first with colorimetric test strips (Merckoquant, Fisher Scientific). Peroxidase in the test field of the strip transfers oxygen to an organic redox indicator that can be analyzed based on a colorimetric visual comparison of the reaction zone with a color scale. For samples that produced H_2O_2, concentration was determined using a variation of the method described by Amonette [17]. A filtered 0.1-mL sample of solution was diluted to 10 mL with distilled water and added to 3 mL of 4.5 M sulfuric acid. This solution was then titrated to the first permanent pink endpoint with 100 μM potassium permanganate that had been prepared and standardized with primary standard grade ferrous ethylenediammonium sulfate $[FeC_2H_4(NH_3)_2(SO_4)_2{\cdot}4H_2O]$ according to the procedure of Diehl [18]. The potassium permanganate was kept in the dark for up to 2 weeks at a time with the concentration being standardized before daily titrations.

3. Results

The synthesized materials were examined by XRD analysis to confirm they were polycrystalline in nature. Fig. 1 shows powder XRD data for the representative materials of (a) PPAM and (b) 5AI. It is seen that both materials exhibit well-defined XRD peaks suggesting the occurence of a polycrystalline phase, with perhaps more than one phase present as illustrated by dual linewidths (only visible upon expanding spectra). Furthermore, the low-angle scattering also supports the assertion of long-range order suggesting that a polymeric structure exists for both materials.

A list of the compounds studied here, their abbreviations, and first-day H_2O_2 concentrations are given in Table 1. In all H_2O_2 production experiments reported here each experiment was run twice to ensure precision, which is confirmed by the agreement to within ±10% in all datasets. Also given is the average photon fractional extinction for the material (A' of Eq. (2)). Of the phenylenediamine (PAM) compounds, only PPAM produced significant H_2O_2. For the diaminopyridine compounds there are three distinct levels of H_2O_2 made. 23DAP and 34DAP each produced 26 mM H_2O_2, 24DAP and 26DAP each made ~6 mM, and 25DAP produced none. Finally, the largest contrast is seen for the aminoindazoles where 5AI made a first-day production of 63 mM/day compared to 6AI that made no H_2O_2.

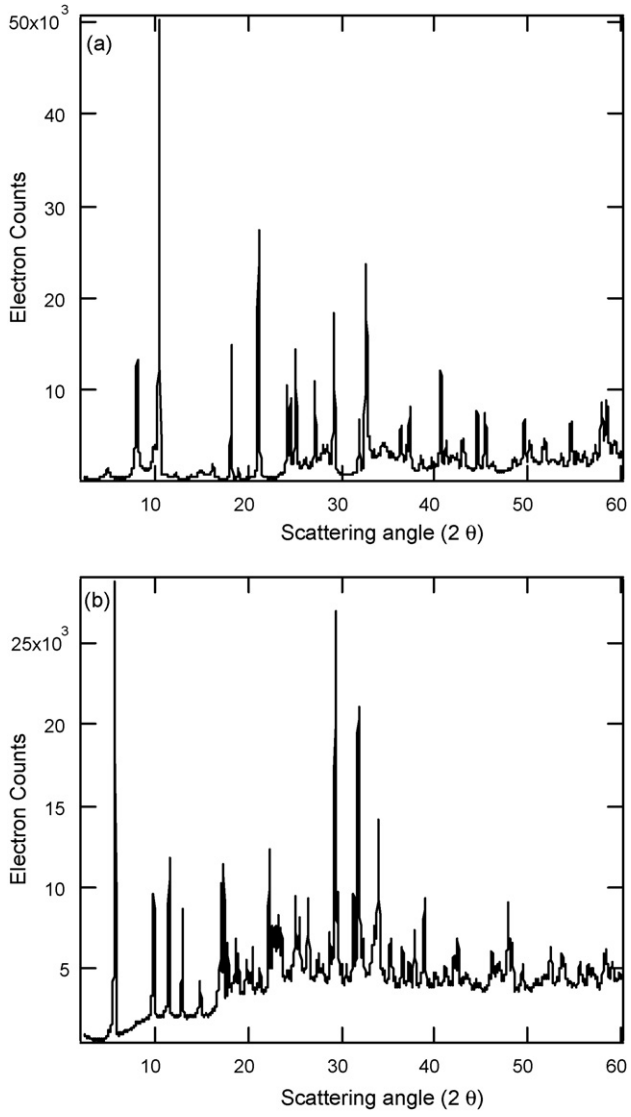

Fig. 1. Powder XRD data are shown for (a) PPAM and (b) 5AI. Note that the well-resolved peaks indicate crystallinity and that the low scattering angle features indicate long-range order exists.

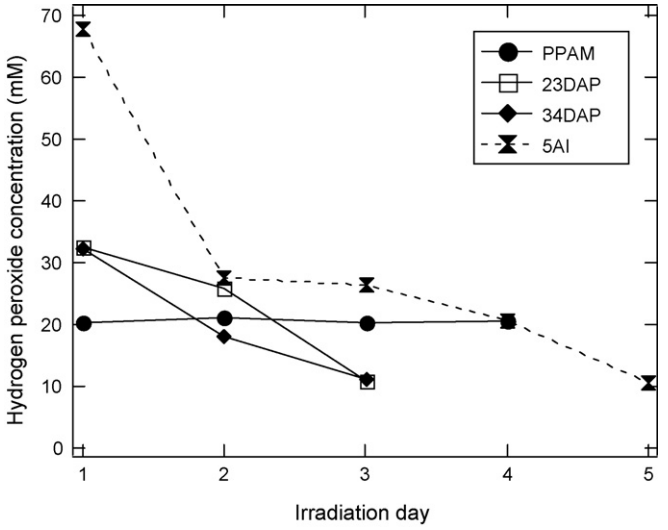

Fig. 2. A plot of the 24-h sampling interval time evolution of H_2O_2 is given for the four compounds: 1,4-phenylenediamine (PPAM); 2,3-diaminopyridine (23DAP); 3,4-diaminopyridine (34DAP); and 5-aminoindazole (5AI). Note that only PPAM has a stable concentration suggesting it may be photocatalytic (and thus without significant material poisoning).

For all the samples where H_2O_2 was produced, experimental runs were also performed by keeping samples in the dark which revealed no H_2O_2 production, thus a true photochemical process was occurring.

An investigation of the H_2O_2 production capability of the materials per irradiation day for the most promising samples is given in Fig. 2. For PPAM a constant H_2O_2 level is seen for days 1–4 at 20 mM. This suggests that little photochemical poisoning is occurring and that its production is likely catalytic with production equal to loss rate processes. Conversely, for 23DAP, and 34DAP a slightly decreasing H_2O_2 level is seen suggesting poisoning of the photocatalyst. Most pronounced, however, is the change between the first-day 5AI H_2O_2 concentration level and subsequent days. Here a large poisoning effect is seen from day 1 to day 2, with a lesser poisoning in subsequent days. Since this result was reproduced this effect is real, but its cause remains unclear.

We calculated a true quantum yield by collecting UV–vis absorbance spectra from which the fraction of light absorbed

Table 1
A list of the compounds studied is given along with the materials' 24-h H_2O_2 production rate, UV–vis reflectivity factor A, and quantum yield Q (see Eqs. (1) and (2) from text)

Compound	24-h rate (mM/day)	Materials' absorbance fraction—A'	Quantum yield—Q (%)
Zinc 1,2-phenylenediamine (12PAM)	0	–	–
Zinc 1,3-phenylenediamine (13PAM)	0	–	–
Zinc *para*-phenylenediamine (PPAM)	18	0.78	14
Zinc 2,4-diaminopyridine (24DAP)	5.6	0.91	3.6
Zinc 2,5-diaminopyridine (25DAP)	0	–	–
Zinc 2,3-diaminopyridine (23DAP)	26	0.92	17
Zinc 2,6-diaminopyridine (26DAP)	7.1	0.91	4.6
Zinc 3,4-diaminopyridine (34DAP)	26	0.97	16
Zinc 6-aminoindazole (6AI)	0	–	–
Zinc 5-aminoindazole (5AI)	63	0.99	37

Zero concentration is below detection limit (<1 mM).

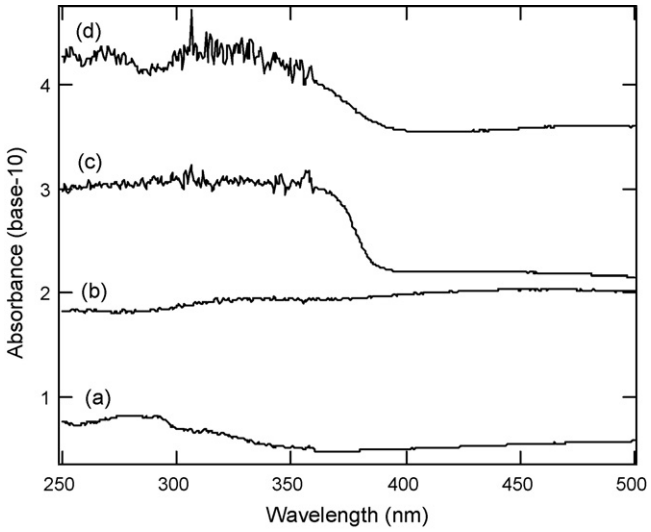

Fig. 3. Absorbance spectra are shown for the four compounds of Fig. 1, namely (a) PPAM, (b) 23DAP, (c) 34DAP, and (d) 5AI. The spectra for (b)–(d) have been offset by 0.8, 1.6, and 2.4 absorbance units, respectively.

by the materials could be computed. Fig. 3 presents data for the compounds examined in Fig. 2 of PPAM (a), 23DAP (b), 34DAP (c), and 5AI (d). It is seen that absorbance from 250 nm to 380 nm increases substantially from (a) to (d). The spectra for (b)–(d) have been offset by 0.8, 1.6, and 2.4 absorbance units for clarity, respectively. Again examining Table 1 the computed A' values and Eq. (2) are used to compute quantum yield Q values. They varied from 3.6% to 37%, with the 5AI value being the largest. In the next section, we rationalize the relative values within a class of compounds for the PAM, DAP, and AI materials.

4. Discussion

As mentioned, the study of irradiated inorganic polymer solids to generate H_2O_2 is novel. Despite this there is related work from which a theoretical interpretation can be proposed. It is likely that upon optical excitation the creation of an electron–hole pair occurs leading to a modestly stable charge-transfer state. This has been discussed in a recent comprehensive review of nanostructured semiconductor materials and donor–acceptor molecular assemblies [19]. This process is most likely to occur by forming an electron localized on the metal site and the hole delocalized on the terminal organic ring moiety of the solid polymer. From this charge-transfer state there are at least two probable reaction outcomes. The first scenario involves a stoichiometric process whereby the formation of H_2O_2 occurs until photocatalyst poisoning occurs. Reactions for this process can be written as follows where M = Zn and LH is the ligand (organic-hydrogen) groups that comprise the

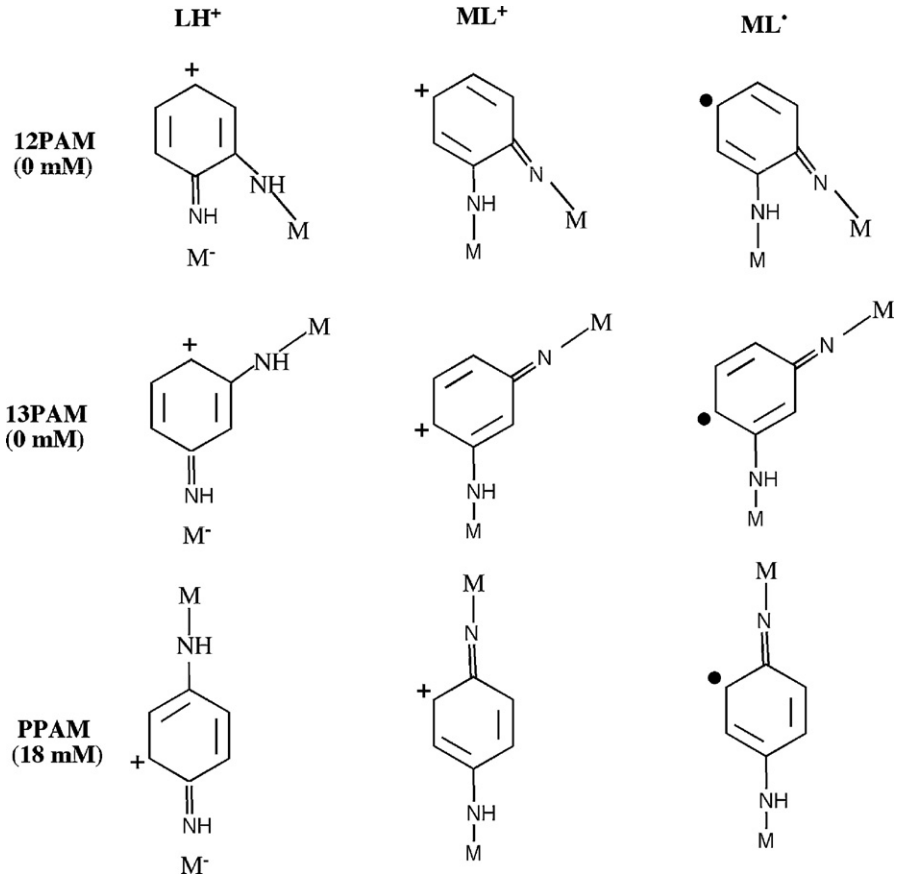

Fig. 4. The LH^+, ML^+, and $ML^\bullet$ resonance structures are shown for phenylenediamine (PAM) compounds. The polymer is constructed by repeating the M–LH (e.g., Zn-PAM) monomer units.

monomer unit within the polymer framework.

$$\text{–M–LH} + h\nu \rightarrow \text{–M}^- + \text{LH}^+ \quad (3a)$$

$$\text{–M}^- + \text{O}_2 \rightarrow \text{–MOO}^- \quad (3b)$$

$$\text{–MOO}^- + \text{H}^+ \rightarrow \text{–MOOH} \quad (3c)$$

$$\text{–MOOH} + \text{LH}^+ \rightarrow \text{–ML}^+ + \text{H}_2\text{O}_2 \quad (3d)$$

$$\text{–ML}^+ + \text{OH}^- \rightarrow \text{–MOH} + \text{L} \quad (3e)$$

$$\text{NET(3a–3e)}: \text{–M–LH} + \text{O}_2 + \text{H}_2\text{O} \rightarrow \text{–MOH} + \text{L} + \text{H}_2\text{O}_2 \quad (3f)$$

Based on the data in Fig. 1 revealing a decreasing H_2O_2 concentration with irradiation day this suggests that the non-catalytic (e.g., poisoned) scenario of these reactions (3a–3e) is applicable to the 23DAP, 34DAP, and 5AI material systems.

The system can be become photocatalytic in one scenario when a MOH + L photoreaction occurs as in reactions (3g) and (3h). Here M–L reacts with water to create a second $OH^\bullet$ radical. The combined photocatalytic H_2O_2 generation process then involves reactions (3a–3e, 3g, 3h) with the net process given as reaction (3i).

$$\text{–MOH} + \text{L} + h\nu \rightarrow \text{–M–L} + \text{OH}^\bullet \quad (3g)$$

$$\text{–M–L} + \text{H}_2\text{O} \rightarrow \text{–M–LH} + \text{OH}^\bullet \quad (3h)$$

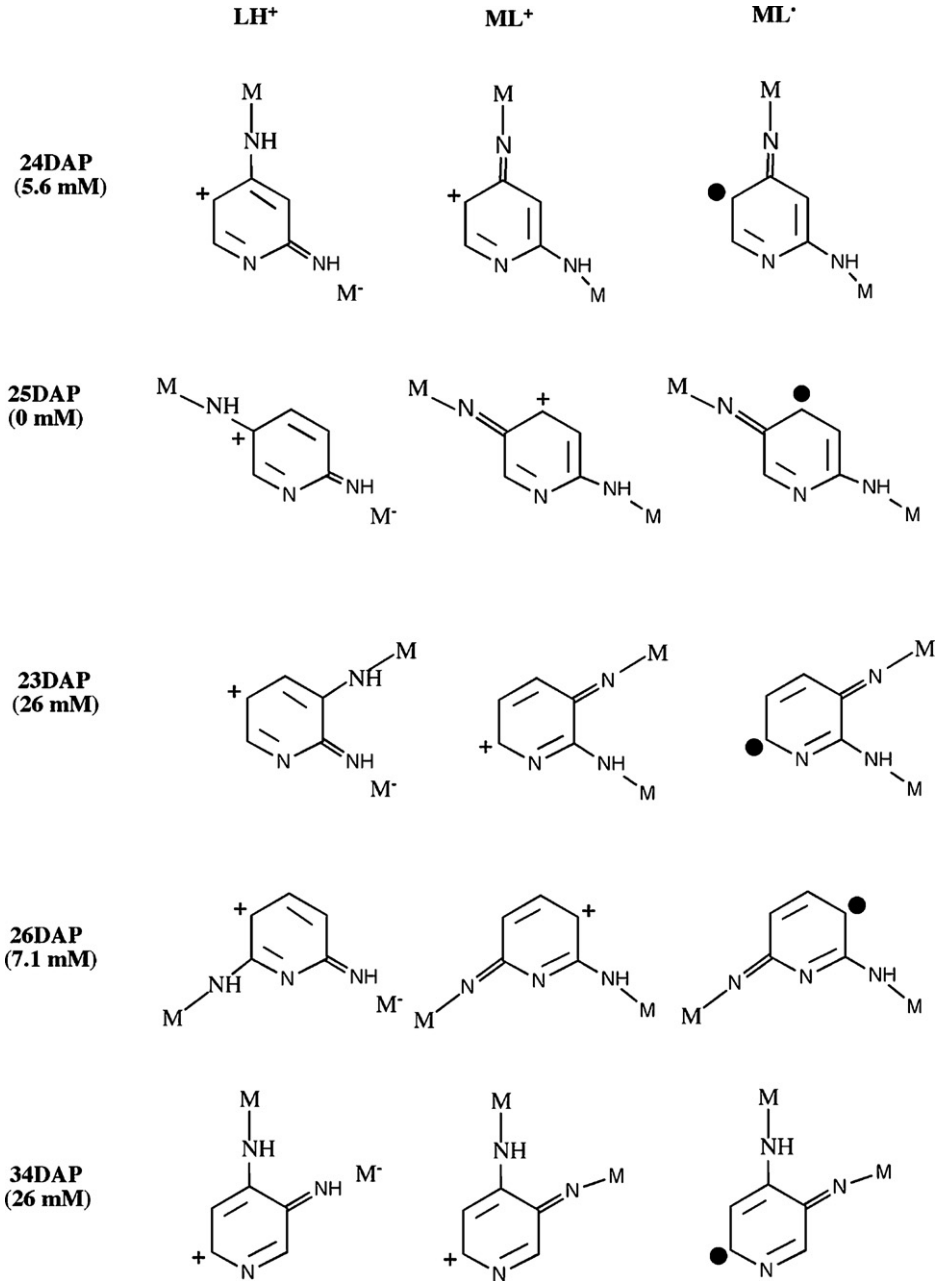

Fig. 5. The LH^+, ML^+, and $ML^\bullet$ resonance structures are shown for diaminopyridine (DAP) polymers. The polymeric solids are constructed by repeating the M–LH (e.g., Zn-DAP) monomer units.

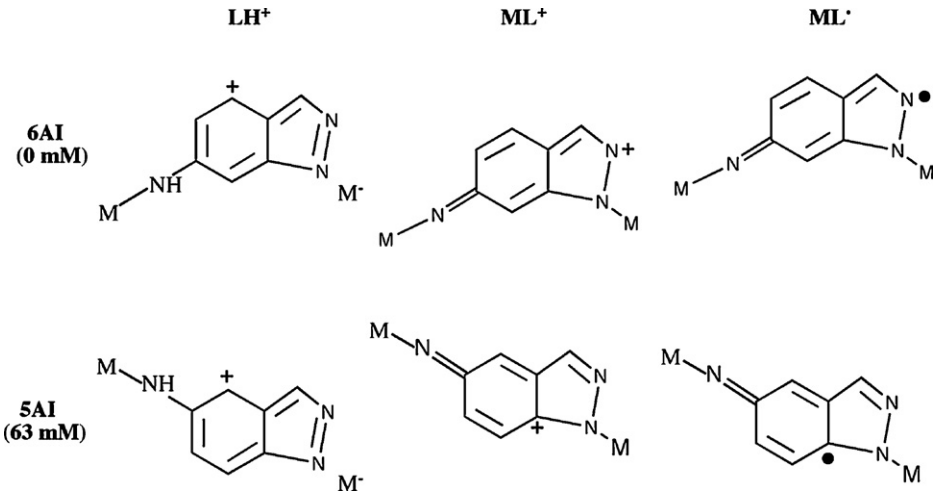

Fig. 6. The LH^+, ML^+, and $ML^\bullet$ resonance structures are shown for aminoindazoles (AI) polymers. Note the significantly more stable ML^+ and $ML^\bullet$ stabilities of 5AI compared to 6AI.

$$\text{NET(3a–3e, 3g, 3h)}: \ O_2 + 2H_2O \ \rightarrow \ 2H_2O_2 \qquad (3i)$$

This photocatalytic set of reactions likely best describes the PPAM system. There exists prior precedence for donor–acceptor hole chemistry for PPAM to act as a hole scavenger when in contact with a CdSe semiconductor [20]. Clearly more work is needed by experimental and computational studies to resolve and assign the stoichiometric/photocatalytic reaction mechanisms given here.

In addition to the general mechanism proposed, it is worthwhile examining at a molecular level the stability of the resonance structures in context of this mechanism to correlate them with the generated first-day H_2O_2 concentrations. Fig. 4 presents the LH^+, ML^+, and $ML^\bullet$ resonance structures for the PAM species. In examining these structures the non-catalytic production of H_2O_2 first occurs via the $LH^+ \rightarrow ML^+$ transition of the first two columns. An identical structure listing is given for the DAP compounds and is presented in Fig. 5. A curious feature is that the first-day H_2O_2 production rate for the PAM compounds are such that the diamino substituent location yields decreasing H_2O_2 production for *para* > *meta* = *ortho* = 0. This is exactly reversed for the DAP structures where *ortho* > *meta* > *para*. An explanation for this, at least in part, may be due to the Bronsted acidity of the PAM compounds (i.e., via the L structures not shown) as compared to the DAP structures. Support for this arises since the pK_a of aniline is 4.6 where the pK_a for 4-aminopyridine is 9.2 [21]. Restated, since the DAP structures are much weaker Bronsted acids than the PAM structures, the DAP non-catalytic H_2O_2 production is best described by L structure instability. It is important to note that in the proposed non-catalytic H_2O_2 production mechanism there are breakages in the polymer chain structure, whereas for the catalytic H_2O_2 production mechanism no net polymer chain cleavage occurs. Therefore the latter will not release ligands into solution. We have indirect support for the breakage of the polymer chains from additional experiments that have revealed that some systems upon irradiation were completely dissolved, albeit with little H_2O_2 production. It is also to be expected that dissolution may result in an increase in alkalinity, something that could be tested for but would not prove or disprove the non-catalytic H_2O_2 production mechanism. An alternative explanation to polymer breakage, such as for bidentate binding organic ligands, is a slippage of the hapticity of the ligand. Future work is needed to study the mechanism in more detail.

A second issue to address is the catalytic production of H_2O_2 for PPAM but not for the DAP materials. The previous paragraph has attempted to present support for chemistry contained in reactions (3a–3d). For the chemistry to be catalytic, it is necessary for reactions (3e, 3g and 3h) to occur. Examining the apparent catalytic nature of PPAM, the much greater π-bonding and resonance stability of pyridine compared to benzene (as analogs) [22] suggests that the DAP stability makes the $ML^\bullet + H_2O$ reaction (reaction (3h)) much less probable for the DAP compared to the PPAM materials.

The remaining system to explore is the aminoindazole (AI) compounds, which are given in Fig. 6. Here the resonance structures clearly seem to explain the reactivity differences between 6AI and 5AI. Again the $LH^+ \rightarrow ML^+$ transition is expected to only be significant for 5AI as the C–N^+–N cation localized structure is much less preferred compared to the C(C)–C^+–C tertiary cation localized structure. Furthermore, the great stability of the 5AI ML^+ structure is exactly what may hinder its hydrolysis (e.g., reaction (3h)) making this otherwise promising material non-catalytic. The stability of this structure is seen though to lead to a threefold enhancement in first-day H_2O_2 production compared to the other systems investigated (see Table 1).

5. Conclusions

We have investigated the photo-production of H_2O_2 on solid polymer Zn(II) complexes in aqueous solutions exposed to the ambient atmosphere. The maximum first-day H_2O_2 production we observed on Zn-5-aminoindazole was 63 mM, which is a factor of ~60 greater than has been seen previously [10,11,14] and translates into an effective quantum yield of 37%. Multi-day

irradiation experiments reveal a constant H_2O_2 concentration for *para*-Zn-phenylenediamine and hence can be photocatalytic in principle. The remaining Zn-diaminopyridines, and Zn-aminoindazoles conversely yield decreasing H_2O_2 concentrations over time, which suggests a poisoning of the photo-activity of the solid materials and that the reaction is not catalytic on the time scale with which we observed the chemistry. Insight into the relative ability of the materials to produce H_2O_2 can be gained by examining their structures. The work here is exploratory in nature and significant study is needed in this promising area of energy research.

Acknowledgements

This project was performed at the *Institute for Interfacial Catalysis* (ICC) at Pacific Northwest National Laboratory (PNNL). The work was carried out in the Environmental Molecular Sciences Laboratory (EMSL) at PNNL, a National Scientific User facility supported by the US Department of Energy Office of Biological and Environmental Research. PNNL is operated by Battelle Memorial Institute for the US Department of Energy. JAH was supported from a Pre-Service Teacher (PST) DOE Office of Fellowship grant.

References

[1] W.T. Hess, Hydrogen peroxide, Kirk-Othmer Encyclopedia of Chemical Technology, vol. 13, 4th ed., Wiley, New York, 1995, pp. 961–995.
[2] Scott, Richard, Homing Instincts, Jane's Navy International (magazine), Alexandria, VA 22314, November 1997.
[3] Hot gas source and fuel, US Patent 4,698,965, October 1987.
[4] The encyclopedia of U-boats: From 1904 to the Present, Eberhard Möller & Werner Brack, Greenhill Books, London, England, February 2006, ISBN: 1853676233.
[5] Hypergolic fuel system, US Patent 6,807,805, October 2004.
[6] W.C. Schumb, C.N. Satterfield, R.L. Wentworth, Hydrogen Peroxide, Am. Chem. Soc. Monograph Series, New York, 1955.
[7] G.H. Miley, N. Luo, J. Mather, R. Burton, G. Hawkins, L. Gu, E. Byrd, R. Gimlin, P.J. Shrestha, G. Benavides, J. Laystrom, D. Carroll, J. Power Sources 165 (2007) 509.
[8] R.K. Raman, N.A. Choudhury, A.K. Shukula, Electrochem. Solid-State Lett. 7 (2004) A488.
[9] P.W. Atkins, Physical Chemistry, 5th ed., W.H. Freeman and Company, New York, 1994.
[10] J.M. Campos-Martin, G. Blanco-Brieva, J.L.G. Fierro, Angew. Chem. Int. Ed. 45 (2006) 6962.
[11] M.C. Markham, K.J. Laidler, J. Phys. Chem. 57 (1953) 363.
[12] M.C. Markham, J.C. Kuriacose, J. DeMarco, C. Giaquinto, J. Phys. Chem. 66 (1962) 932.
[13] M.C. Markham, M.C. Hannan, L. Lin, C. Coffey, B. Jones, J. Phys. Chem. 62 (1958) 989.
[14] A.J. Hoffman, E.R. Carraway, M.R. Hoffmann, Environ. Sci. Technol. 28 (1994) 776.
[15] B.J. Finlayson-Pitts, J.N. Pitts Jr., Chemistry of the Upper and Lower Atmosphere: Theory, Experiments and Applications, Academic Press, New York, 2000.
[16] J.E. Bauman Jr., J.C. Wang, Inorg. Chem. 3 (1963) 368.
[17] J.E. Amonette, The role of structural iron oxidation in the weathering of trioctahedral micas by aqueous solutions, Ph.D. Dissertation, Iowa State University, Ames, IA, pp.102–103, 1988.
[18] H. Diehl, Quantitative Analysis: Elementary Principles and Practice, Oakland Street Science Press, Ames, IA, 1974, pp. 229–230.
[19] P.V. Kamat, J. Phys. Chem. B 111 (2007) 2834.
[20] S.N. Sharma, Z.S. Pillai, P.V. Kamat, J. Phys. Chem. B 107 (2003) 10088.
[21] C. Zhou, Y. Jin, J.R. Kenseth, M. Stella, K.R. Wehmeyer, W.R. Heineman, J. Pharm. Sci. 94 (3) (2005) 576.
[22] I. Fernandez, G. Frenking, Faraday Discuss. 135 (2007) 403.